

## Article

# PVA-Based MMMs for Ethanol Dehydration via Pervaporation: A Comparison Study between Graphene and Graphene Oxide

Xia Zhan <sup>1,\*</sup>, Rui Ge <sup>1</sup>, Zhongyong Gao <sup>1</sup>, Teng Gao <sup>1</sup>, Luying Wang <sup>2</sup> and Jiding Li <sup>3</sup>

<sup>1</sup> Key Laboratory of Cleaner Production and Integrated Resource Utilization of China National Light Industry, Beijing Technology and Business University, Beijing 100048, China; geruixx@163.com (R.G.); gaozhongyong2020@163.com (Z.G.); skybluesunny2022@163.com (T.G.)

<sup>2</sup> Beijing Key Laboratory of Lignocellulosic Chemistry, Beijing Forestry University, Beijing 100083, China; wangly@bjfu.edu.cn

<sup>3</sup> Department of Chemical Engineering, Tsinghua University, Beijing 100084, China; lijiding@mail.tsinghua.edu.cn

\* Correspondence: zhanxia@th.btbu.edu.cn

**Abstract:** Two different types of 2D nanosheets, including hydrophobic graphene (GR) and hydrophilic graphene oxide (GO), were filled into poly (vinyl alcohol) (PVA) polymers to prepare mixed matrix membranes (MMMs) for ethanol dehydration via pervaporation. The relationship between the physical/chemical properties of graphene and pervaporation performance of MMMs was investigated by a comparison of GR/PVA and GO/PVA MMMs in microstructure and PV performance. The incorporation of GO nanosheets into PVA reduced PVA crystallinity and enhanced the membrane hydrophilicity, while the incorporation of GR into PVA led to the opposite results. The incorporation of GR/GO into PVA depressed the PVA membrane swelling degree, and the incorporation of GR showed a more obvious depression effect. GR/PVA MMMs showed a much higher separation factor than GO/PVA MMMs, while they exhibited a much lower permeation flux than GO/PVA MMMs and pristine PVA membranes. The huge difference in microstructure and performance between GO/PVA and GR/PVA MMMs was strongly associated with the oxygen-containing groups on graphene lamellae. The higher permeation flux of GO/PVA MMMs was ascribed to the facilitated transport of water molecules induced by oxygen-containing groups and exclusive channels provided by GO lamellae, while the much lower permeation flux and higher separation factor GR/PVA MMMs was resulted from the smaller GR interplanar spacing (0.33 nm) and hydrophobicity as well as barrier effect of GR lamellae on the sorption and diffusion of water molecules. It was presumed that graphene intercalated with an appropriate number of oxygen-containing groups might be a good choice to prepare PVA-based MMMs for ethanol dehydration, which would combine the advantages of GR's high interlayer diffusion selectivity and GO's high permeation properties. The investigation might open a door to achieve both of high permeation flux and separation factor of PVA-based MMMs by tuning the microstructure of graphene.

**Keywords:** graphene; graphene oxide; poly (vinyl alcohol); mixed matrix membrane; ethanol dehydration; pervaporation



**Citation:** Zhan, X.; Ge, R.; Gao, Z.; Gao, T.; Wang, L.; Li, J. PVA-Based MMMs for Ethanol Dehydration via Pervaporation: A Comparison Study between Graphene and Graphene Oxide. *Separations* **2022**, *9*, 26. <https://doi.org/10.3390/separations9020026>

Academic Editor: Piotr Paweł Wiecek

Received: 24 December 2021

Accepted: 18 January 2022

Published: 21 January 2022

**Publisher's Note:** MDPI stays neutral with regard to jurisdictional claims in published maps and institutional affiliations.



**Copyright:** © 2022 by the authors. Licensee MDPI, Basel, Switzerland. This article is an open access article distributed under the terms and conditions of the Creative Commons Attribution (CC BY) license (<https://creativecommons.org/licenses/by/4.0/>).

## 1. Introduction

Ethanol dehydration via pervaporation (PV) has attracted increasing attention due to the rapid development and application of ethanol biofuel [1–3]. Membrane is the key factor in the PV process to achieve high separation performance. When dealing with the ethanol dehydration, hydrophilic polymers are the most commonly used membrane materials [4–17], and the PVA membrane is the only one to realize industrial application due to its high hydrophilicity, good solubility in water, excellent film-forming property, biodegradability, and eco-friendly properties [18]. However, the PV performance of pristine PVA membranes showed a trade-off effect between permeability and selectivity. One

of the most effective methods for improving the PV performance of PVA membranes is the incorporation of inorganic fillers into polymers to fabricate mixed matrix membranes (MMMs) [19–24]. MMMs can combine the advantages of inorganic fillers and polymeric membranes to ideally achieve an enhanced synergistic separation performance. To date, plenty of PVA-based MMMs have been developed for ethanol dehydration, and the inorganic fillers commonly used were including zeolite [25–27], silica [28], carbon nanotubes (CNT) [29–31], metal–organic frameworks (MOFs) [32–35], and other hydrophilic inorganic materials [19–22,36,37].

Recently, graphene (GR) and its derivatives, especially graphene oxide (GO) nanosheets, have attracted great attention due to the unique 2D nanochannels for ultra-fast and selective molecular transport [38–40]. The poor compatibility of graphene with polar polymers is unfavorable for the development and applications of GR-based composite materials [41]. Compared with GR, GO nanosheets are highly oxygenated with oxygen-containing groups on their basal planes and sheet edges, such as hydroxyl, epoxy, and carboxyl groups. Benefiting from these oxygen-containing groups, GO shows much better compatibility with polar polymers than GR, which makes GO an excellent nanofiller for the PVA polymers. However, the investigation on the graphene/PVA MMMs for ethanol dehydration up to now is still very limited. Moreover, the relationship between the physical/chemical properties of graphene and pervaporation performance of MMMs is unclear, which makes it difficult to choose an appropriate graphene type to effectively enhance the PV performance of PVA membranes.

In this work, two typical graphene nanosheets, including hydrophobic GR and hydrophilic GO, as shown in Figure 1, were incorporated into a PVA matrix to achieve better performance for ethanol dehydration. To the best of our knowledge, there is no report about the comparison between GR/PVA and GO/PVA MMMs for ethanol dehydration via pervaporation. The effect of graphene type (GR and GO) on the membrane microstructure, hydrophilicity, and swelling properties as well as the pervaporation dehydration performance of PVA-based MMMs were investigated in detail, which might give some insight for the design of PVA-based MMMs with high ethanol dehydration performance by tuning the graphene microstructure.

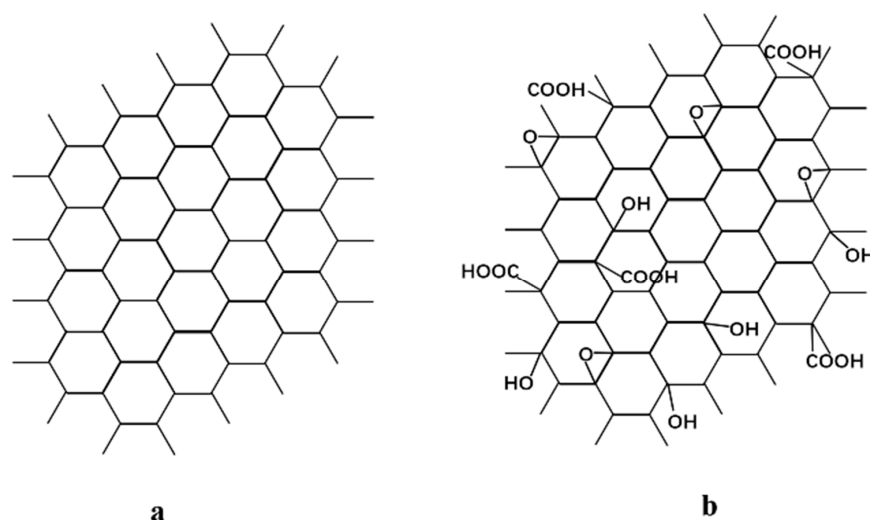


**Figure 1.** Chemical structure of (a) graphene and (b) graphene oxide.

## 2. Materials and Methods

### 2.1. Materials

Polyacrylonitrile (PAN, MW = 150,000) was provided by DuPont. PVA (1799) was bought from Shanghai Aladdin Biochemical Technology Co., Ltd., Shanghai, China. Graphene oxide (GO) and graphene (GR) nanosheets were purchased from Nanjing XFNANO Materials Tech Co., Ltd, Nanjing, China. *N,N'*-dimethylformamide (DMF) was bought from Fuchen

Chemical Reagent Co., Ltd., Tianjin, China, glutaraldehyde (GA, 50 wt% aqueous solution) was provided by Shanghai Maclean Biochemical Technology Co., Ltd., Shanghai, China. Sulfuric acid ( $\text{H}_2\text{SO}_4$ ) and ethanol were received from Sinopharm Group Chemical Reagent Co., Ltd., Shanghai, China. Deionized water was made in the laboratory.

### 2.2. Preparation of PAN Porous Membranes

PAN porous membranes were fabricated by the phase inversion method. PAN powder (56 g) was dissolved in DMF solvent (344 g) with vigorous stirring at 80 °C until a homogeneous solution was obtained. The solution was filtered to remove impurities and insoluble components, and then, it was defoamed for 3 h to remove the bubbles. Then, the PAN aqueous solution was cast at a speed of 1.2 m/min on a PET non-woven fabric using a membrane scraper (HOLYKEM, Suzhou, China) set at a gap of 150  $\mu\text{m}$ . The resulting membrane was immediately immersed in the nonsolvent coagulation bath (deionized water) at 20 °C. The fresh membranes were washed every 4 h. After 48 h, the porous PAN membranes were dried at 30 °C for use.

### 2.3. Preparation of PVA-Based MMMs

The PVA-based MMMs were fabricated by blending fillers and PVA polymer in solution and casting on PAN porous support, as shown in Figure 2. PVA powder was dissolved under vigorous mechanical stirring in deionized water at 90 °C to form 10 wt% PVA aqueous solution. GR/GO fillers were dispersed in deionized water with magnetic stirring for 30 min and ultrasonication for 30 min to obtain a homogeneous suspension or solution. An appropriate amount of PVA solution and filler suspension were mixed together and processed by stirring (30 min each) and sonication twice (30 min each). Afterwards, the pH of solution was adjusted to 2 with  $\text{H}_2\text{SO}_4$ . Then, the pre-crosslinking of PVA was initiated by adding GA to the dope, which was stirred for another 20 min and cast on a porous PAN substrate or PTFE plate. The degree of crosslinking (X), which was defined as the mole ratio of GA to PVA repeat unit, was controlled at 1%. The fresh MMMs were heated at 50 °C for 3 h and subsequently deeply crosslinked at 70 °C for 3 h. The chemical crosslinking of PVA with GA is shown in Figure S1. To make comparison with MMMs, pure PVA membrane crosslinked by GA was also prepared via a similar process. The filler loading was defined as the mass ratio of filler to PVA, which was 0.5 wt%, 1 wt%, and 2 wt%, respectively.

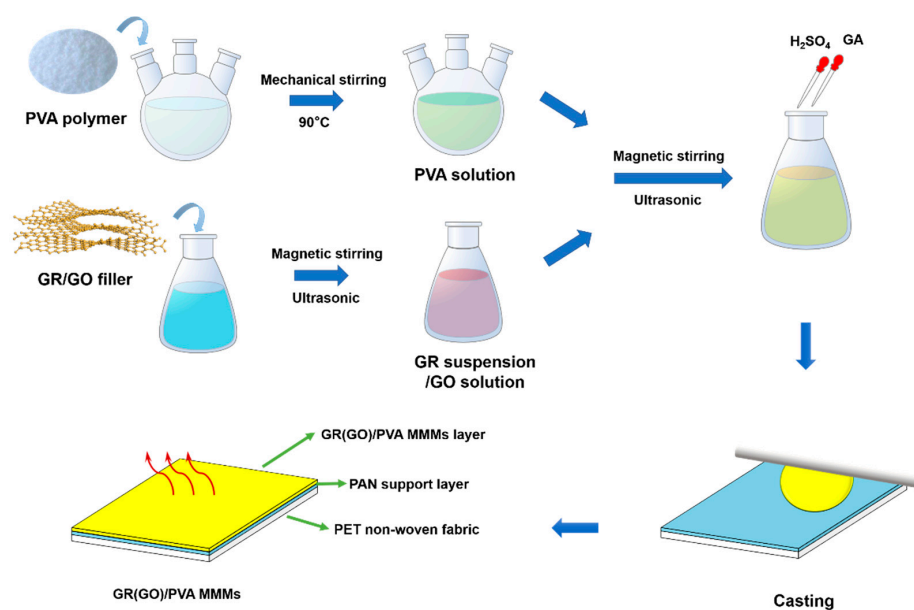


Figure 2. Preparation process of PVA-based MMMs.

### 2.4. Characterization

The morphology and microstructure of MMMs were characterized by field emission scanning electron microscopy (SEM, JSM-7410, Nippon Electric Industry Corporation, Tokyo, Japan). The chemical and crystalline structure of MMMs were characterized using a Fourier transform infrared spectrometer (FT-IR, Nicolet iS10 iSO10, Thermo Fisher Scientific Corporation, Waltham, MA, USA) and X-ray diffractometer (D8 Advance, Bruker, Germany). The static contact angle of water on the sample surface was determined using a contact angle meter (OCA-20, Dataphysics, Germany) at room temperature. The swelling degree was measured at 40 °C with 90 wt% ethanol/water mixtures. The thermal properties of MMMs were characterized by a TGA analyzer (STA409C/3/F, Netzsch, Germany).

### 2.5. Pervaporation Performance Measurement

The pervaporation performance was evaluated with a homemade apparatus, as shown in Figure S2 [42]. The membrane area was 0.0022 m<sup>2</sup>. The circulating ethanol aqueous solution was in contact with one side of the membrane, which was selectively permeated across the membrane and condensed in the flasks. The pressure at the permeate side was controlled below 500 Pa, and the feed side was operated under ordinary pressure. Ethanol concentration in the feed and permeate was measured by gas chromatography (GC7900, Techcomp, Shanghai, China). The ethanol feed concentration varied in the range of 75–90 wt%, and the temperature varied from 40 to 70 °C. The permeate flux *J* and separation factor  $\alpha$  was used to evaluate the PV performance as follows [43].

$$\alpha = \frac{y_W/y_E}{x_W/x_E}$$

where *W* and *E* is water and ethanol; *x* and *y* denote the mass fraction of ethanol/water in the feed and permeate, respectively. The permeation flux *J* can be calculated according to the following equation:

$$J = \frac{Q}{t \cdot A}$$

where *Q* represents the total quantity of the permeate through the membrane area *A* in time *t*.

Membrane flash index (MFLI) [44,45] is another simple and valuable method to evaluate the PV membranes' capabilities in liquid separation compared to traditional distillation, which is mainly based on the comparison of available theoretical maximum distillate compositions.

$$MFLI = \frac{y_i^{PV}}{y_i^D[VLE]}$$

where *y*<sub>*i*</sub><sup>PV</sup> is the permeate concentration (wt%) and *y*<sub>*i*</sub><sup>D</sup>[VLE] is the equilibrium distillation value (wt%).

Permeability (*P*<sub>*i*</sub>) and membrane selectivity ( $\beta$ ) were obtained according to the following equations [43]:

$$P_i = J_i \times \frac{l}{x_i \gamma_i P_i^{sat} - y_i P^p}$$

$$\beta = \frac{P_W}{P_E}$$

where *P*<sub>*i*</sub> was the permeation coefficient of component *i*; *l* is the thickness of the membrane selective layer; *x*<sub>*i*</sub> and *y*<sub>*i*</sub> denote the molar fraction of component *i* in the feed and permeate, respectively;  $\gamma_i$  is the activity coefficient of the component in the feed; *P*<sub>*i*</sub><sup>sat</sup> is the saturation vapor pressure of the pure component *i*; and *P*<sup>p</sup> denotes the total pressure on the permeate side, which can be treated as zero when the permeation test is under vacuum conditions.

### 3. Results

#### 3.1. Characterization of PVA-Based MMMs

##### 3.1.1. Chemical Structures of PVA-Based MMMs

Elemental analysis was carried out to determine C and O elemental compositions of GR/GO fillers, as shown in Table 1. The elemental oxygen content of GR was only 1.2 wt%, while that of GO reached as high as 46.9 wt%. This suggested that GR almost entirely consisted of carbon elements, while GO sheets possessed plenty of oxygen-containing functional groups, which contributed to its high oxidation degree. The FT-IR characterization also confirmed this conclusion.

**Table 1.** Elemental analysis for GR and GO.

Sample	C (wt%)	O (wt%)	H (wt%)	Oxidation Degree (%)
GR	98.1	1.2	0.6	0.9
GO	46.3	46.9	1.9	75.9

The FT-IR spectra of PVA-based MMMs with different filler loading was exhibited in Figure 3. The FT-IR spectrum of GO showed the presence of hydroxyl ( $3440\text{ cm}^{-1}$ ), epoxy ( $1227\text{ cm}^{-1}$ ), and carbonyl ( $1738\text{ cm}^{-1}$ ) groups [46]. The bands at  $3439\text{ cm}^{-1}$  corresponded to the stretching vibration of -OH, which might be ascribed to the adsorbed water on GR, and the stretching vibration of  $\text{sp}^2\text{ C}=\text{C}$  was found at  $1627\text{ cm}^{-1}$  [47]. The main characteristic absorption peak at  $3268\text{ cm}^{-1}$  was attributed to the OH stretching of the pure PVA membrane. The relative intensity of absorption peaks at  $1086\text{ cm}^{-1}$  and  $1141\text{ cm}^{-1}$  was indicative of the semi-crystalline nature of the polymer composites [48]. Compared with pristine PVA membranes, both GR/PVA and GO/PVA MMMs exhibited similar features with a shift of the characteristic peak at  $3268\text{ cm}^{-1}$  to  $3266\text{ cm}^{-1}$  and  $3264\text{ cm}^{-1}$ , respectively. The red shift of the characteristic peak could be ascribed to the interfacial interactions between the filler and PVA. The red shift in GO/PVA MMMs was more significant than that in GR/PVA MMMs due to the strong hydrogen bonding formed between the oxygen-containing groups on the GO nanosheets and the -OH groups of PVA. A similar phenomenon was also found by other researchers. Kashyap et al. [48] reported that the incorporation of GO into PVA resulted in a more significant red shift of the -OH characteristic peak than that of reduced GO, which was ascribed to the larger amount of polar groups on the GO sheets than those on the reduced GO sheets enhancing the interfacial interaction between the PVA and the GO nanosheets.

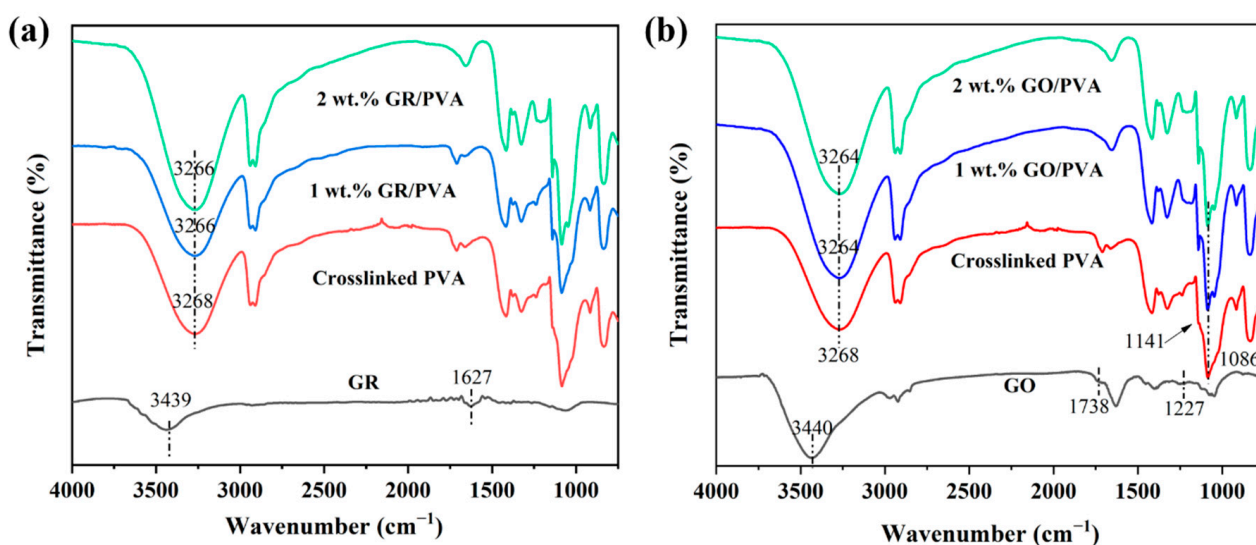


**Figure 3.** FT-IR spectra of GR/PVA MMMs (a) and GO/PVA MMMs (b).

### 3.1.2. Crystal Structures of PVA-Based MMMs

Figure 4 shows XRD spectra for crosslinked PVA, GO, GR, and PVA-based MMMs. The strong diffraction peak of crosslinked PVA at  $2\theta = 19.92^\circ$  was attributed to the crystalline plane of (1 0 1) and (2 0 0) mixtures of PVA [49]. GR showed a strong diffraction peak at  $2\theta = 26.55^\circ$ , and the corresponding interplanar spacing of GR was only 0.33 nm due to the strong  $\pi$ - $\pi$  interaction between GR lamellae [41]. The GR interplanar spacing (0.33 nm) was exactly in between the kinetic diameters of ethanol and water molecules, which was 0.43 nm and 0.26 nm, respectively [45]. This might facilitate the selective permeation of water molecules. As expected, GO showed a diffraction band at  $2\theta = 12.03^\circ$ , which suggested that the interplanar spacing of the GO lamellae was enlarged to 0.74 nm by oxygen-containing functional groups on GO nanosheets [46].

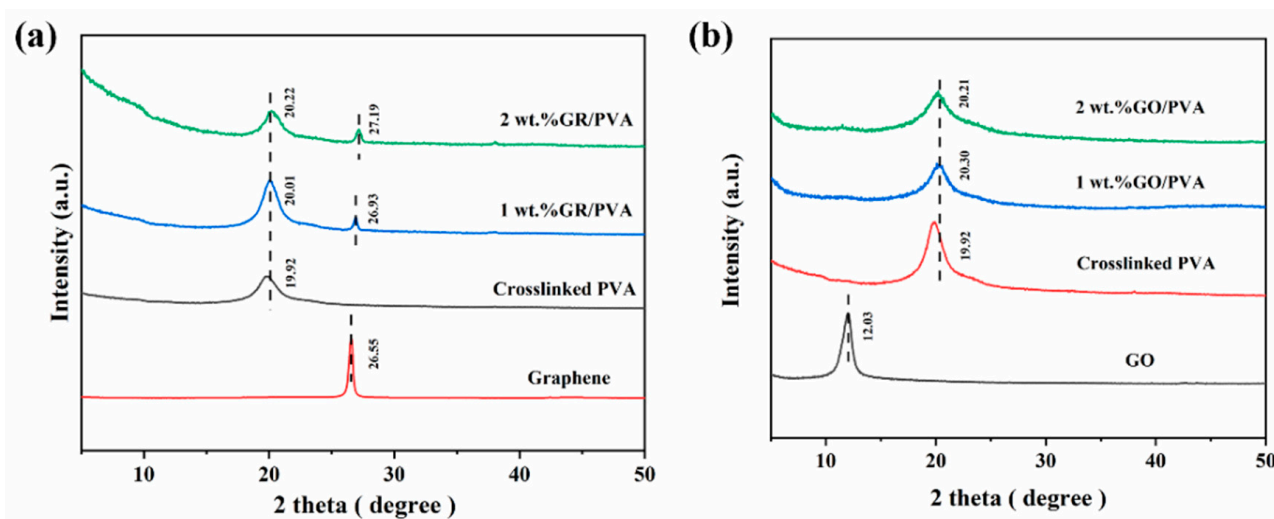


Figure 4. XRD patterns of GR, GR/PVA MMMs (a) and GO, GO/PVA MMMs (b) with different filler loading.

It was shown that the intensities of PVA diffraction peaks declined with the incorporation of GO into the PVA matrix, and the diffraction peak of GO almost disappeared in MMMs. This indicated that the PVA crystallinity decreased, and the GO nanosheet was well exfoliated and homogeneously dispersed in the PVA matrix, which was mainly ascribed to the strong interaction that exists between the PVA polymer and GO nanosheets. On the contrary, the incorporation of GR into PVA increased the intensity of the PVA diffraction peak, and an obvious diffraction peak of GR in MMMs was observed, which might be resulted from the weak interaction between GR aggregates and PVA polymers. As GR loading increased from 0 wt% to 2 wt%, the diffraction angles of PVA and GR increased, which suggested that the interplanar spacing of both crystalline PVA and GO lamellae decreased slightly.

### 3.1.3. Morphology of PVA-Based MMMs

The surface and cross-section morphology of PVA-based MMMs with different filler loading are presented in Figures 5 and 6. The pure crosslinked PVA showed a relatively smooth and dense surface morphology, as shown in Figure 5. The incorporation of GO into PVA increased the surface roughness of MMMs slightly, and GO was well covered by PVA polymer chains even with 2 wt% filler loading. The compact and almost smooth surface of GO/PVA MMMs indicated the homogeneous dispersion of GO and the strong interaction between GO and PVA, which was consistent with the FT-IR and XRD results. Compared with GO/PVA MMMs, GR/PVA MMMs exhibited a compact surface with clusters and protrusion scattered on the membrane surface, which might result from the aggregation of GR in the PVA matrix and weak interfacial interaction between GR and PAV. As GR loading increased, the GR aggregation became obvious on the surface of MMMs. In cross-sectional

view, all the selective layers in MMMs were bonded with the PAN support layer tightly. No obvious filler aggregation was observed in the cross-section of GR/PVA or GO/PVA MMMs. It was found that GO lamellae were arranged almost horizontally in the PVA matrix, while the arrangement direction of GR was inconspicuous.

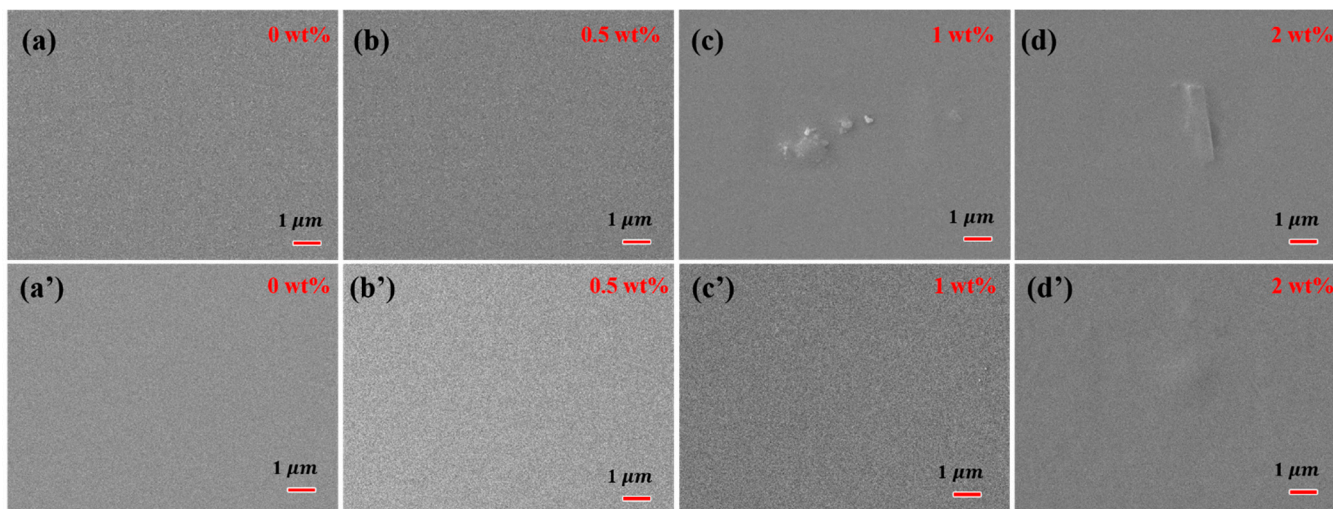


**Figure 5.** Surface morphology of GR/PVA MMMs (up) and GO/PVA MMMs (down). (a,a') pure PVA membrane; (b,b') filler loading of 0.5 wt%; (c,c') filler loading of 1 wt%; (d,d') filler loading of 2 wt%.

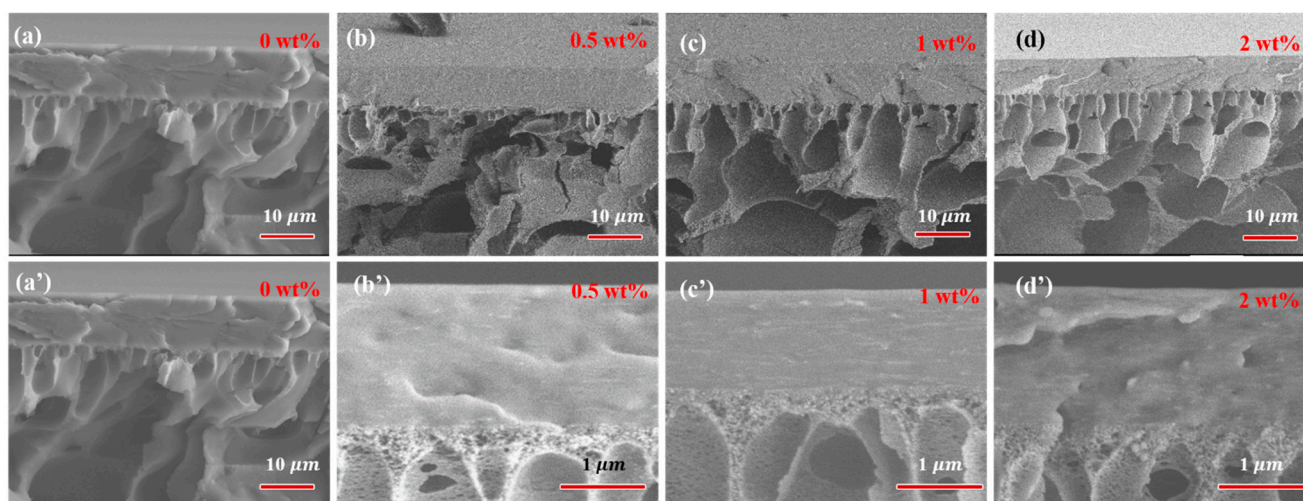


**Figure 6.** Cross-section morphology of GR/PVA (up) and GO/PVA MMMs (down). (a,a') pure PVA membrane; (b,b') filler loading of 0.5 wt%; (c,c') filler loading of 1 wt%; (d,d') filler loading of 2 wt%.

### 3.1.4. Hydrophilicity of PVA-Based MMMs

Water contact angles analysis for PVA-based MMMs membranes with different GR/GO loading is exhibited in Figure 7. The water contact angle of the pure crosslinked PVA membrane was  $63^\circ$ , which showed hydrophilic property. An interesting phenomenon was found in which the incorporation of GR and GO filler into the PVA matrix exhibited the opposite effect on the surface hydrophilicity of PVA membranes. As the GR/GO filler loading increased, the water contact angle of the GR/PVA MMMs increased sharply from  $63^\circ$  to  $85^\circ$ , while that of GO/PVA MMMs decreased from  $63^\circ$  to  $57^\circ$ . This might be attributed to the intrinsic hydrophobicity of GR and hydrophilicity of GO filler as well as the higher surface roughness of GR/PVA MMMs, as observed in SEM. The increased hydrophilicity of GO/PVA MMMs might be in favor of the enhancement of water sorption in membranes.

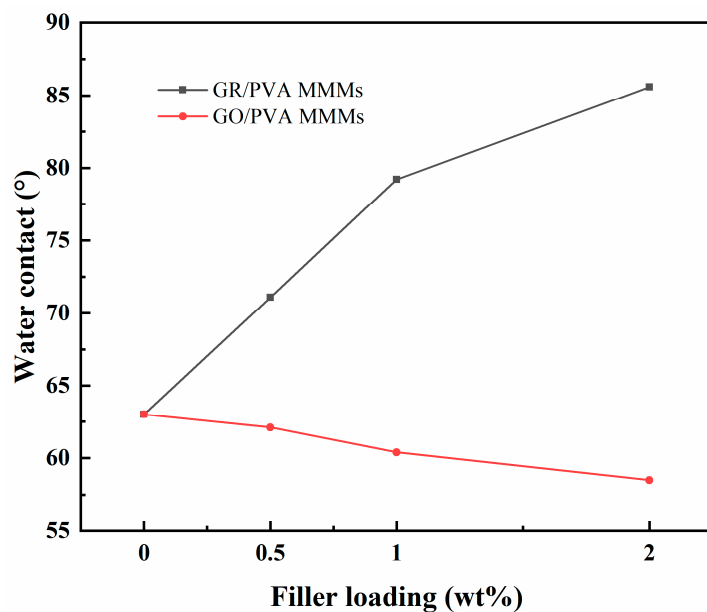


Figure 7. Effect of filler loading on contact angles of GR/PVA and GO/PVA MMMs.

### 3.1.5. Swelling Properties of PVA-Based MMMs

The swelling degrees of the pristine PVA membrane and PVA-based MMMs in 90 wt% ethanol aqueous solution at 40 °C are shown in Figure 8. Compared with the pure PVA membrane, both GR/PVA and GO/PVA MMMs showed much lower swelling degrees, and the swelling degree of GR/PVA MMMs decreased more sharply than that of GO/PVA MMMs with increasing filler loading. This was mainly attributed to the increased hydrophobicity and PVA crystallinity of the GR/PVA MMMs, as confirmed by the water contact angles and XRD results. The decrease in swelling degree with the augment of GO loading might be attributed to the strong hydrogen bonding between GO nanosheets and PVA polymers, which restrained the mobility of PVA chains. Although the incorporation of GO into the PVA matrix enhanced the surface hydrophilicity of PVA slightly, the restraining effect of GO on PVA chain mobility might play a more important role and resulted in the decrease in swelling degree.

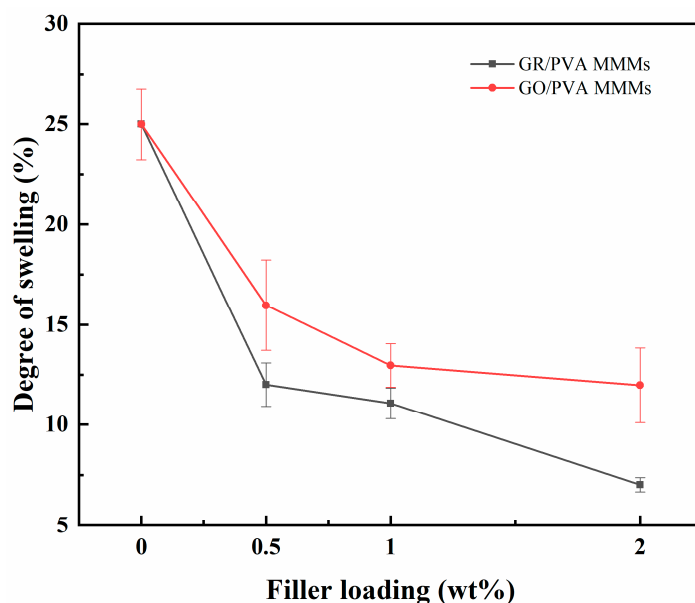


Figure 8. Effect of filler loading on swelling degree of GR/PVA and GO/PVA MMMs.

### 3.1.6. Thermal Properties of PVA-Based MMMs

The thermal stability of membrane materials was evaluated by TGA, as shown in Figure S3. GR showed good stability, with weight loss of only 7.0 wt% in the range of 25–800 °C. GO exhibited a first gradual weight loss (14%) before 150 °C, which resulted from the loss of the water molecules that were confined in its structure. The second weight loss that started at 200 °C was presumably due to pyrolysis of the oxygen-containing functional groups on GO nanosheets [18]. This weight loss corresponded to 28% by weight of the total material. The last weight loss that started at 580 °C was ascribed to the combustion process. The pristine PVA membrane and GR/PVA as well as GO/PVA MMMs showed similar degradation properties, with a three-stage weight loss. In the first stage, the weight loss of PVA-based MMMs started at about 50 °C, which was mainly attributed to the evaporation of free water molecules absorbed in the membrane. The second weight loss between 150 and 220 °C generally resulted from the water bonded to PVA via hydrogen bonding and the partial degradation of GO. GO/PVA MMMs showed larger weight loss than the pure PVA membrane in this temperature range, while GR/PVA MMMs exhibited smaller weight loss than the pure PVA membrane, which might be ascribed to more water molecules being adsorbed in GO/PVA MMMs due to its hydrophilicity and the partial degradation of GO. The third weight loss between 360 and 470 °C was presumably due to pyrolysis of the crosslinked PVA chains [50]. Both GR/PVA and GO/PVA MMMs showed higher degradation residues weight than PVA, which suggested that the incorporation of GR or GO into PVA improved the thermal stability of PVA at high temperature.

## 3.2. Pervaporation Performance of PVA-Based MMMs

### 3.2.1. Effect of GR/GO Filler Loading on PV Performance

Figure 9 showed the effect of GR/GO filler loading on the PV performance of PVA based MMMs with 90 wt% ethanol/water mixtures at 40 °C. With the augment of filler loading, the separation factor of both GR/PVA MMMs and GO/PVA MMMs increased first and subsequently decreased, which reached the maximum values of 1400 and 481, respectively, with 1 wt% filler loading, increasing by 402% and 72% compared with the pure PVA membrane. The permeation flux of GO/PVA MMMs increased, while that of GR/PVA MMMs decreased with the augment of filler loading. The different variation tendency in PV performance with filler loading might be associated with the intrinsic hydrophobicity/hydrophilicity of fillers and membrane surface, interplanar spacing of fillers, PVA crystallinity, and the interfacial interaction in MMMs. The ethanol/water permeation mechanism across GR/PVA and GO/PVA MMMs is proposed in Figure 10. As for GR/PVA MMMs, the hydrophobic GR surface and smaller interplanar spacing (0.33 nm) as well as increased PVA crystallinity was unfavorable for the adsorption and diffusion of small molecules, which showed a barrier effect for ethanol/water molecules, as illustrated in channel 1 and 2. Molecules permeated through the zigzag pathways as shown in channel 3, which resulted in the decrease in both ethanol and water flux. Moreover, as the kinetic diameter of the ethanol molecule was larger than that of the water molecule, the barrier effect might have a more obvious influence on ethanol permeation, which contributed to the high separation factor. In addition, the proper GR interplanar spacing (0.33 nm), which was exactly in between the kinetic diameters of ethanol and water molecules (0.43 nm and 0.26 nm, respectively), might contribute to the selective permeation of water molecules and resulted in a much higher separation factor. As for GO/PVA MMMs, GO was well exfoliated by PVA and arranged almost horizontally in the PVA matrix. The much larger interplanar spacing and hydrophilic surface of GO lamellae as well as the decreased PVA crystallinity might provide more and larger transport pathways for small molecules, which effectively enhanced the permeation flux. On the one hand, the oxygen-containing groups on GO lamellae might facilitate the adsorption and diffusion of water molecules due to the hydrogen bonding between GO and water molecules. Although the transport pathways around the zigzag GO lamellae seemed to be prolonged, the permeation of water molecules was facilitated due to the strong

interaction between GO and water molecules. On the other hand, the GO lamellae stacking might result in two types of slit pores between adjacent GO lamellae in the horizontal direction, as shown in Figure 10. Type I allows ethanol and water permeation, while type II only permits water permeation. The facilitated transport of water molecules induced by oxygen-containing groups and exclusive channels for water molecules provided by slit pores between adjacent GO lamellae might contribute to the both higher separation factor and permeation flux than that of the pure PVA membrane.

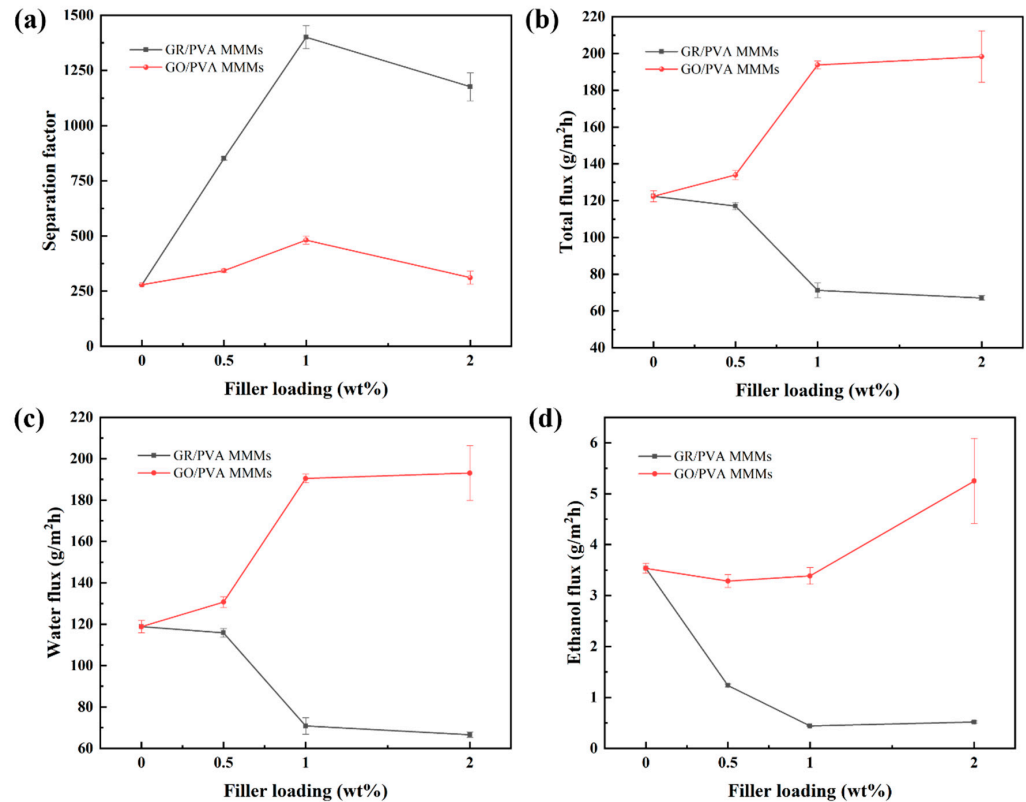


Figure 9. Effect of filler loading on PV performance of GR/PVA and GO/PVA MMMs. (a) Separation factor; (b) Total flux; (c) Water partial flux; (d) Ethanol partial flux.

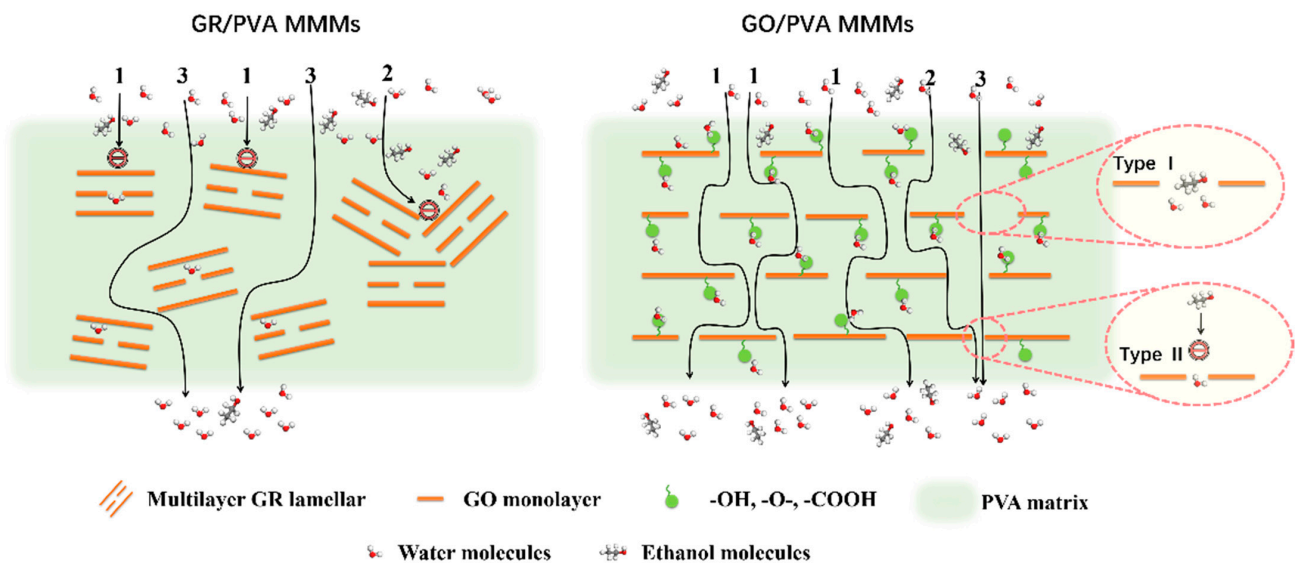


Figure 10. Schematic diagram of the hypothetical ethanol/water permeation mechanism across GR/PVA and GO/PVA MMMs.

### 3.2.2. Effect of Feed Concentration on PV Performance

The effect of ethanol concentration on the PV performance of PVA-based MMMs is shown in Figure 11. It was found that the separation factor increased, while the total flux and ethanol/water partial flux of both GR/PVA and GO/PVA MMMs decreased with ethanol concentration increasing from 75 wt% to 90 wt%. It might be ascribed to the variation in membrane swelling and driving force as well as cluster formation with increasing feed concentration. On the one hand, as the water content in the solution decreased, the swelling degree of the MMMs decreased due to the water affinity of MMMs, which was unfavorable to the permeation of small molecules. Since water molecules possess a smaller kinetic diameter than ethanol molecules, the decline of ethanol flux was more significant than that of water flux. On the other hand, the driving force for ethanol transport increased, while that for water transport decreased with the augment of ethanol feed concentration (as shown in Table S1). This might contribute to the enhancement of ethanol flux and decline of water flux. In addition, the formation of water–water, ethanol–ethanol, and water–ethanol clusters via hydrogen bonding also had a significant impact on permeation flux. Since clusters possessed larger kinetic diameters and resulted in reduced diffusivity, ethanol clusters suffered more than water clusters [51]. The increased ethanol concentration might lead to more and larger ethanol clusters, which resulted in the greatly reduced diffusivity of ethanol molecules. Conversely, the lower water concentration might weaken the coupling effect of water molecules, which contributed to the increase in water diffusivity due to the small sizes of water molecules and its clusters. The several opposite factors mentioned above competed together and finally resulted in the decrease in total flux and enhancement of separation factor with increasing ethanol concentration. As shown in Figure S4, the ethanol and water permeability decreased with increasing ethanol concentration, and the membrane selectivity increased significantly. This suggested that the variation of intrinsic membrane microstructure with increasing ethanol concentration was unfavorable for the permeation of small molecules but was beneficial to the improvement of membrane selectivity.

### 3.2.3. Effect of Operation Temperature on PV Performance

As shown in Figure 12, the PV performance GR/PVA MMMs showed the similar variation trend with that of GO/PVA with temperature increasing from 40 to 70 °C (ethanol concentration of 90 wt%). The total flux of PVA-based MMMs increased with raising the operation temperature, and the separation factor followed the reversed order. This may be attributed to the following reasons: (1) Increasing temperature enhanced the membrane swelling and the mobility of PVA chains, creating more and larger free volume available for small molecules [42], which might contribute to the improvement of permeability; (2) The driving force, which was strongly related to the saturated vapor pressure, was significantly improved due to the increased saturation vapor pressure with feed temperature rising, as shown in Table S2 [45]. (3) The diffusion coefficient of ethanol/water molecules increased with the temperature rising as reported in many studies in the literature [43,52], which also resulted in the increase in total flux.

According to the Arrhenius equation, it was found that the variation of the permeation flux of PVA-based MMMs with increasing feed temperature followed the Arrhenius relationship. The apparent permeation activation energy was 52.70 and 83.81 kJ/mol for water and ethanol flux in the 1.0 wt% GR/PVA MMMs, while it was 43.06 and 58.53 kJ/mol for water and ethanol flux in the 1.0 wt% GO/PVA MMMs. The apparent permeation activation energy for water and ethanol flux in GR/PVA MMMs was much higher than those in GO/PVA MMMs especially for ethanol flux, which indicated that the permeation resistance in GR/PVA MMMs was higher than that in GO/PVA MMMs. This led to the much lower permeation flux of GR/PVA MMMs than that of GO/PVA MMMs. Moreover, the ethanol permeation activation energy was larger than the water permeation activation energy, which suggested that the ethanol permeation was more sensitive to the operation temperature than water permeation in PVA based MMMs. As the operation temperature

increased, the growth of ethanol flux was more significant than that of water flux, which led to a lower separation factor.

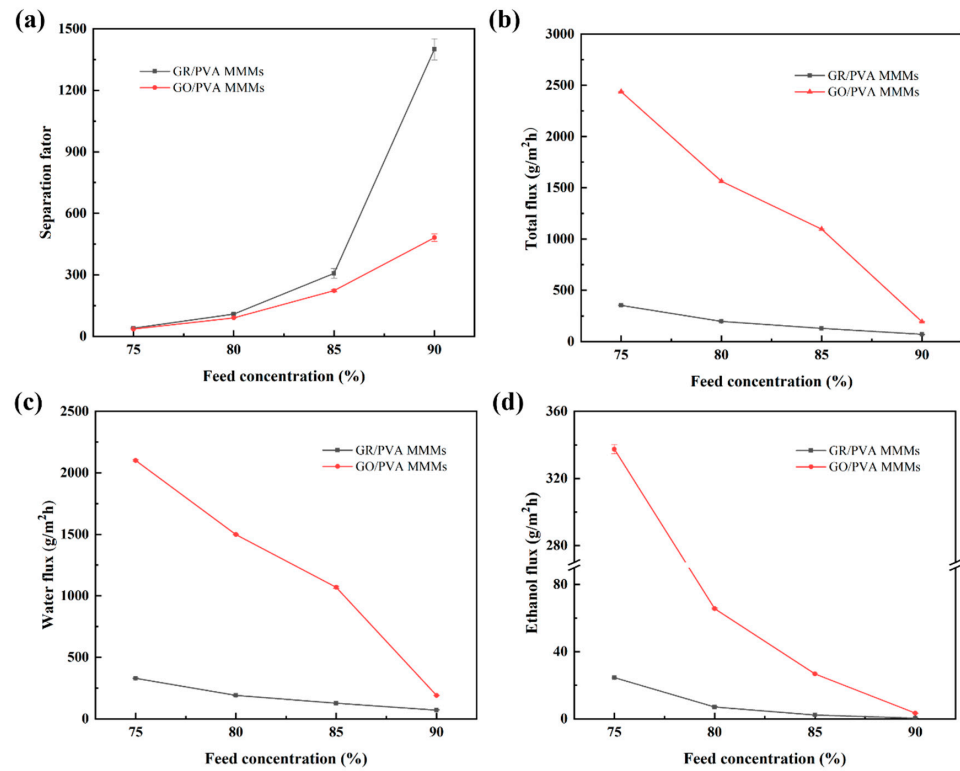


**Figure 11.** Effect of ethanol concentration on PV performance of GR/PVA and GO/PVA MMMs: (a) Separation factor; (b) Total flux; (c) Water partial flux; (d) Ethanol partial flux.

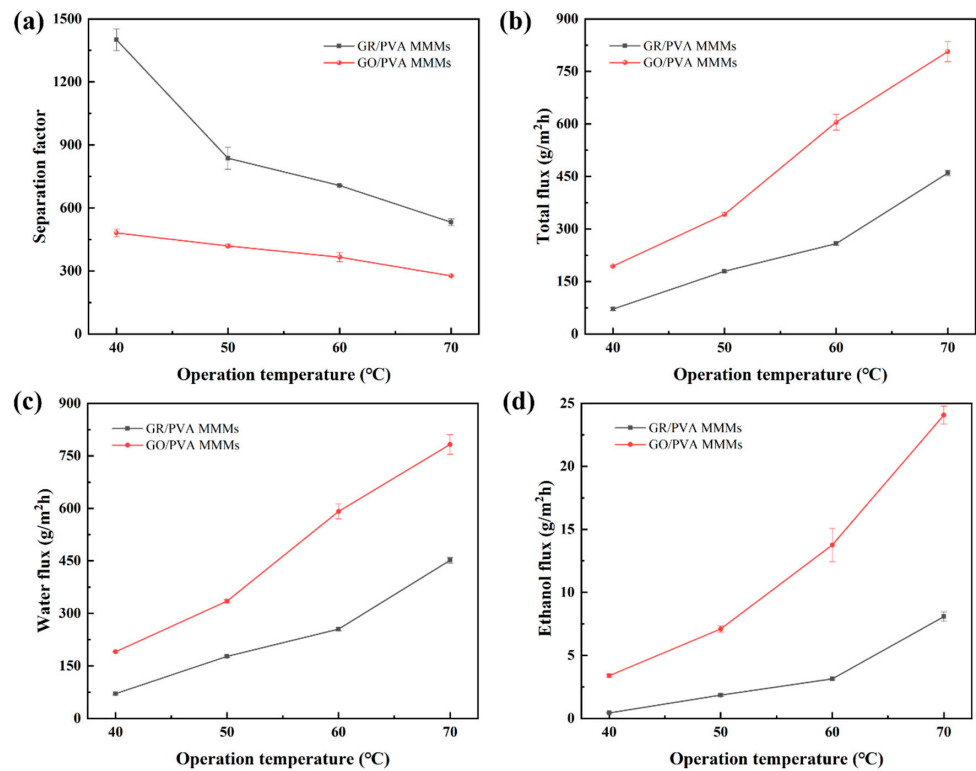


**Figure 12.** Effect of operation temperature on PV performance of GR/PVA and GO/PVA MMMs: (a) Separation factor; (b) Total flux; (c) Water partial flux; (d) Ethanol partial flux.

### 3.2.4. Comparison of PV Performance of PVA-Based MMMs

The performance of PVA-based MMMs for ethanol dehydration via PV strongly depended on (i) the PVA polymer characteristics (e.g., molecular weight, alcoholysis degree, crosslinking conditions, etc.); (ii) the filler features (e.g., type, size, hydrophilicity/hydrophobicity, shape, morphology); and (iii) the operating conditions (e.g., ethanol feed concentration, operation temperature, feed flow rate, vacuum pressure) [1]. This made it difficult to fairly compare the PV data of PVA-based MMMs, which made it challenging to select the best performance of PVA-based MMMs. To evaluate the overall performance of a membrane, it was useful to evaluate their separation ability by means of PSI. The water–ethanol PV separation performances of PVA-based MMMs filled with different inorganic fillers are listed Table 2. It was found that the PVA-based MMMs prepared in this work displayed better PSI values in comparison to other PVA-based MMMs reported in the literature. GR/PVA MMMs exhibited the highest separation factor of 1400 and lower permeation flux than other PVA-based MMMs due to the hydrophobic properties and lower interplanar spacing of GR. GO/PVA MMMs showed higher permeation flux with a considerable separation factor due to the homogeneous dispersion and hydrophilic properties of the GO monolayer. MFLI was also used to evaluate the PV membranes' capabilities in liquid separation compared to traditional distillation. It can be seen that the graphene/PVA MMMs prepared in this work exhibited comparable or even higher MFLI values compared with other PVA-based MMMs reported in the literature, which indicated that pervaporation with these MMMs possessed better separation efficiency over flash distillation [44,45]. According to the results, it was presumed that graphene intercalated with an appropriate number of oxygen-containing groups might be a good choice to prepare PVA-based MMMs for ethanol dehydration, which would combine the advantages of GR's high interlayer diffusion selectivity and GO's high permeation properties and open a door to achieve both high permeation flux and the separation factor of MMMs by tuning the microstructure of graphene.

**Table 2.** PV performance of PVA-based MMMs for ethanol dehydration.

Membrane	Filler Loading (wt%)	Feed Temperature (°C)	Ethanol Concentration (wt%)	Total Flux (g/m <sup>2</sup> h)	Separation Factor	PSI (kg/m <sup>2</sup> h)	MFLI	Ref.
Zirconia/PVA	42	50	90	105	142	14.8	10.45	[20]
silica/PVA	2	30	90	40	180	7.2	10.58	[27]
H-ZSM-5/PVA	7	30	96	125–118	349–236	43.5–27.7	22.69–23.39	[25]
Zeolite X/PVA	5	30	90	374	178	66.2	10.58	[26]
c-alumina/PVA	-	50	90	330	56	18.2	9.57	[21]
CNT/PVA	1	40	90	82	460	37.6	10.90	[28]
CNT/PVA	5	30	90	50	780	39.0	10.98	[30]
CNT/PVA	5	40	90	80	500	39.9	10.91	[30]
ZIF-90/PVA	-	30	90	268	1379	369.3	11.04	[33]
ZIF-8-NH <sub>2</sub> /PVA	7.5	40	85	120	200	23.9	10.80	[31]
AgNP/PVA	0.5	50	90	89	101.7	9.0	10.21	[23]
UiO-66/PVA	8	30	90	979	2084	2039.3	11.06	[34]
rGO/PVA	0.3	50	80	56	51.2	2.8	10.31	[36]
GO/PVA	2	70	90	185	65.9	12.0	9.78	[19]
GO/PVA	1	40	90	137	263	35.9	10.74	[19]
GO/PVA	1	40	90	194	481	93.1	10.91	This work
GR/PVA	1	40	90	71	1400	99.3	11.04	This work
GR/PVA	1	50	90	179	837	149.6	10.99	This work

## 4. Conclusions

The relationship between the physical/chemical properties of graphene and pervaporation performance of MMMs was investigated by comparison of GR/PVA and GO/PVA MMMs in microstructure and PV performance.

- (1) GR lamellae were dispersed in the PVA matrix in the form of multilayer aggregates due to the strong  $\pi$ - $\pi$  interaction between GR layers and weak interaction between GR and PVA. GO was well exfoliated by PVA and homogeneously dispersed in the

PVA matrix, benefiting from the good solubility of GO, and a strong interaction existed between the GO nanosheet and PVA polymer due to oxygen-containing groups. The incorporation of GO nanosheets into PVA reduced PVA's crystallinity and enhanced the membrane hydrophilicity, while the incorporation of GR into PVA led to the opposite results. The incorporation of GR/GO into PVA depressed the PVA membrane swelling degree, and the incorporation of GR showed a more obvious depression effect.

- (2) GR/PVA MMMs showed a much higher separation factor than GO/PVA MMMs, while they exhibited much lower permeation flux than GO/PVA MMMs and pristine PVA membranes. The huge difference in microstructure and performance between GO/PVA and GR/PVA MMMs was strongly associated with the oxygen-containing groups on graphene lamellae. The higher permeation flux of GO/PVA MMMs was ascribed to the facilitated transport of water molecules induced by oxygen-containing groups and exclusive channels provided by GO lamellae, while the much lower permeation flux and higher separation factor GR/PVA MMMs resulted from the smaller GR interplanar spacing (0.33 nm) and hydrophobicity as well as barrier effect of GR lamellae on the sorption and diffusion of water molecules. With the augment of filler loading, the separation factor of both GR/PVA MMMs and GO/PVA MMMs increased first and subsequently decreased, which reached maximum values of 1400 and 481 respectively at 1 wt% filler loading, increasing by 402% and 72% compared with that of the pristine PVA membrane.
- (3) The pervaporation performance of GR/PVA MMMs showed similar variation trends with that of GO/PVA as the water feed concentration or operation temperature increased. As the operation temperature or water feed concentration increased, the separation factor decreased, while the total flux and ethanol/water partial flux increased.

**Supplementary Materials:** The following supporting information can be downloaded at <https://www.mdpi.com/article/10.3390/separations9020026/s1>, Figure S1: Chemical crosslinking of PVA with GA; Figure S2: The pervaporation apparatus; Figure S3: The TG curves for GR/PVA MMMs (a) and GO/PVA MMMs (b); Figure S4: Effect of ethanol feed concentration on PV performance of GR/PVA and GO/PVA MMMs (a) Membrane selectivity; (b) Permeability; Table S1: Effect of feed concentration on activity coefficient, saturated vapor pressure, and feed fugacity at 40 °C; Table S2: Effect of feed temperature on activity coefficient, saturated vapor pressure, and feed fugacity of ethanol/water (90 wt%) mixture.

**Author Contributions:** Data collation, R.G. and T.G.; formal analysis, R.G. and T.G.; funding acquisition, X.Z., J.L. and L.W.; investigation, R.G., T.G. and Z.G.; methodology, R.G. and T.G.; project management, X.Z.; writing—original draft, R.G. and X.Z.; writing—reviewing and editing, X.Z. All authors have read and agreed to the published version of the manuscript.

**Funding:** The authors greatly appreciate the financial support of Beijing Natural Science Foundation Commission-Beijing Municipal Education Commission Joint Foundation, China (KZ201910011012), National Natural Science Foundation of China (21736001, 21206001), Open Research Fund Program of Key Laboratory of Cleaner Production and Integrated Resource Utilization of China National Light Industry (No. CP-2020-YB7) and Graduate research capability improvement program of Beijing Technology and Business University (2022020).

**Institutional Review Board Statement:** Not applicable.

**Informed Consent Statement:** Not applicable.

**Data Availability Statement:** Exclude this statement.

**Conflicts of Interest:** There are no conflict of interest to declare.

## References

1. Zhu, T.; Xia, Q.; Zuo, J.; Liu, S.; Yu, X.; Wang, Y. Recent advances of thin film composite membranes for pervaporation applications: A comprehensive review. *Adv. Membr.* **2021**, *1*, 100008. [[CrossRef](#)]
2. Lin, G.-S.; Chen, Y.-R.; Chang, T.-H.; Huang, T.-C.; Zhuang, G.-L.; Huang, W.-Z.; Liu, Y.-C.; Matsuyama, H.; Wu, K.C.W.; Tung, K.-L. A high ZIF-8 loading PVA mixed matrix membrane on alumina hollow fiber with enhanced ethanol dehydration. *J. Membr. Sci.* **2021**, *621*, 118935. [[CrossRef](#)]
3. Liu, G.; Jin, W. Pervaporation membrane materials: Recent trends and perspectives. *J. Membr. Sci.* **2021**, *636*, 119557. [[CrossRef](#)]
4. Li, M.; Wang, J.; Zhou, S.; Xue, A.; Wu, F.; Zhao, Y. Polyacrylonitrile-supported self-aggregation crosslinked poly (vinyl alcohol) pervaporation membranes for ethanol dehydration. *Eur. Polym. J.* **2020**, *122*, 109359. [[CrossRef](#)]
5. Thorat, G.B.; Gupta, S.; Murthy, Z.V.P. Synthesis, characterization and application of PVA/ionic liquid mixed matrix membranes for pervaporation dehydration of isopropanol. *Chin. J. Chem. Eng.* **2017**, *25*, 1402–1411. [[CrossRef](#)]
6. Dmitrenko, M.E.; Penkova, A.V.; Missyul, A.B.; Kuzminova, A.I.; Markelov, D.A.; Ermakov, S.S.; Roizard, D. Development and investigation of mixed-matrix PVA-fullerenol membranes for acetic acid dehydration by pervaporation. *Sep. Purif. Technol.* **2017**, *187*, 343–354. [[CrossRef](#)]
7. Zhang, S.Y.; Zou, Y.; Wei, T.Y.; Mu, C.X.; Liu, X.J.; Tong, Z.F. Pervaporation dehydration of binary and ternary mixtures of n-butyl acetate, n-butanol and water using PVA-CS blended membranes. *Sep. Purif. Technol.* **2017**, *173*, 314–322. [[CrossRef](#)]
8. Li, S.; Dai, J.; Geng, X.; Li, J.; Li, P.; Lei, J.; Wang, L.; He, J. Highly selective sodium alginate mixed-matrix membrane incorporating multi-layered MXene for ethanol dehydration. *Sep. Purif. Technol.* **2020**, *235*, 116206. [[CrossRef](#)]
9. Nigiz, F.U.; Dogan, H.; Hilmioglu, N.D. Pervaporation of ethanol/water mixtures using clinoptilolite and 4A filled sodium alginate membranes. *Desalination* **2012**, *300*, 24–31. [[CrossRef](#)]
10. Lecaros, R.L.G.; Ho, S.-Y.; Tsai, H.-A.; Hung, W.-S.; Hu, C.-C.; Huang, S.-H.; Lee, K.-R.; Lai, J.-Y. Ionically cross-linked sodium alginate and polyamidoamine dendrimers for ethanol/water separation through pervaporation. *Sep. Purif. Technol.* **2021**, *275*, 119125. [[CrossRef](#)]
11. Kononova, S.V.; Kruchinina, E.V.; Petrova, V.A.; Baklagina, Y.G.; Klechkovskaya, V.V.; Orekhov, A.S.; Vlasova, E.N.; Popova, E.N.; Gubanov, G.N.; Skorik, Y.A. Pervaporation membranes of a simplex type with polyelectrolyte layers of chitosan and sodium hyaluronate. *Carbohydr. Polym.* **2019**, *209*, 10–19. [[CrossRef](#)]
12. Silvestre, W.P.; Baldasso, C.; Tessaro, I.C. Potential of chitosan-based membranes for the separation of essential oil components by target-organophilic pervaporation. *Carbohydr. Polym.* **2020**, *247*, 116676. [[CrossRef](#)]
13. Xu, Y.M.; Japip, S.; Chung, T.-S. Mixed matrix membranes with nano-sized functional UiO-66-type MOFs embedded in 6FDA-HAB/DABA polyimide for dehydration of C1-C3 alcohols via pervaporation. *J. Membr. Sci.* **2018**, *549*, 217–226. [[CrossRef](#)]
14. Xu, S.; Wang, Y. Novel thermally cross-linked polyimide membranes for ethanol dehydration via pervaporation. *J. Membr. Sci.* **2015**, *496*, 142–155. [[CrossRef](#)]
15. Le, N.L.; Wang, Y.; Chung, T.S. Synthesis, cross-linking modifications of 6FDA-NDA/DABA polyimide membranes for ethanol dehydration via pervaporation. *J. Membr. Sci.* **2012**, *415–416*, 109–121. [[CrossRef](#)]
16. Shi, G.M.; Yang, T.; Chung, T.S. Polybenzimidazole (PBI)/zeolitic imidazolate frameworks (ZIF-8) mixed matrix membranes for pervaporation dehydration of alcohols. *J. Membr. Sci.* **2012**, *415–416*, 577–586. [[CrossRef](#)]
17. Shi, G.M.; Chen, H.M.; Jean, Y.C.; Chung, T.S. Sorption, swelling, and free volume of polybenzimidazole (PBI) and PBI/zeolitic imidazolate framework (ZIF-8) nano-composite membranes for pervaporation. *Polymer* **2013**, *54*, 774–783. [[CrossRef](#)]
18. Castro-Muñoz, R.; Buera-González, J.; Iglesia, Ó.D.L.; Galiano, F.; Fila, V.; Malankowska, M.; Rubio, C.; Figoli, A.; Téllez, C.; Coronas, J. Towards the dehydration of ethanol using pervaporation cross-linked poly (vinyl alcohol)/graphene oxide membranes. *J. Membr. Sci.* **2019**, *582*, 423–434. [[CrossRef](#)]
19. Tsebriienko, T.; Popov, A.I. Effect of Poly (Titanium Oxide) on the Viscoelastic and Thermophysical Properties of Interpenetrating Polymer Networks. *Crystals* **2021**, *11*, 794. [[CrossRef](#)]
20. Peters, T.; Benes, N.; Buijs, H.; Vercauteren, F.; Keurentjes, J. Thin high flux ceramic-supported PVA membranes. *Desalination* **2006**, *200*, 37–39. [[CrossRef](#)]
21. Chaudhari, S.; Baek, M.; Kwon, Y.; Shon, M.; Nam, S.; Park, Y. Surface-modified halloysite nanotube-embedded polyvinyl alcohol/polyvinyl amine blended membranes for pervaporation dehydration of water/isopropanol mixtures. *Appl. Surf. Sci.* **2019**, *493*, 193–201. [[CrossRef](#)]
22. Selim, A.; Toth, A.J.; Fozer, D.; Haaz, E.; Valentínyi, N.; Nagy, T.; Keri, O.; Bakos, L.P.; Szilágyi, I.M.; Mizsey, P. Effect of silver-nanoparticles generated in poly (vinyl alcohol) membranes on ethanol dehydration via pervaporation. *Chin. J. Chem. Eng.* **2019**, *27*, 1595–1607. [[CrossRef](#)]
23. Park, H.B.; Kamcev, J.; Robeson, L.M.; Elimelech, M.; Freeman, B.D. Maximizing the right stuff: The trade-off between membrane permeability and selectivity. *Science* **2017**, *356*, eaab0530. [[CrossRef](#)]
24. Nguyen, H.H.; To, L.A.; Ngo, N.P. Fabrication and characterization of graphene/graphene oxide based poly (vinyl alcohol) nanocomposite membranes for pervaporation dehydration of ethanol. *Can Tho. Univ. J. Sci.* **2016**, *36–45*, Special issue: Renewable Energy. [[CrossRef](#)]
25. Suhas, D.P.; Aminabhavi, T.M.; Raghu, A.V. Mixed matrix membranes of H-ZSM5-loaded poly (vinyl alcohol) used in pervaporation dehydration of alcohols: Influence of silica/alumina ratio. *Polym. Eng. Sci.* **2014**, *54*, 1774–1782. [[CrossRef](#)]

26. Asvadi, F.; Raisi, A.; Aroujalian, A. Preparation of multi-layer pervaporation membrane by electrospraying of nano zeolite X. *Microporous Mesoporous Mater.* **2017**, *251*, 135–145. [[CrossRef](#)]
27. Huang, Z.; Ru, X.-f.; Zhu, Y.-T.; Guo, Y.-h.; Teng, L.-j. Poly (vinyl alcohol)/ZSM-5 zeolite mixed matrix membranes for pervaporation dehydration of isopropanol/water solution through response surface methodology. *Chem. Eng. Res. Des.* **2019**, *144*, 19–34. [[CrossRef](#)]
28. Samei, M.; Iravaninia, M.; Mohammadi, T.; Asadi, A.A. Solution diffusion modeling of a composite PVA/fumed silica ceramic supported membrane. *Chem. Eng. Process.* **2016**, *109*, 11–19. [[CrossRef](#)]
29. Choi, J.H.; Jegal, J.; Kim, W.N. Modification of performances of various membranes using MWNTs as a modifier. *Macromol. Symp.* **2007**, *249–250*, 610–617. [[CrossRef](#)]
30. Panahian, S.; Raisi, A.; Aroujalian, A. Multilayer mixed matrix membranes containing modified-MWCNTs for dehydration of alcohol by pervaporation process. *Desalination* **2015**, *355*, 45–55. [[CrossRef](#)]
31. Choi, J.H.; Jegal, J.; Kim, W.-N.; Choi, H.-S. Incorporation of multiwalled carbon nanotubes into poly (vinyl alcohol) membranes for use in the pervaporation of water/ethanol mixtures. *J. Appl. Polym. Sci.* **2009**, *111*, 2186–2193. [[CrossRef](#)]
32. Zhang, H.; Wang, Y. Poly (vinyl alcohol)/ZIF-8-NH<sub>2</sub> mixed matrix membranes for ethanol dehydration via pervaporation. *AIChE J.* **2016**, *62*, 1728–1739. [[CrossRef](#)]
33. Wei, Z.; Liu, Q.; Wu, C.; Wang, H.; Wang, H. Viscosity-driven in situ self-assembly strategy to fabricate cross-linked ZIF-90/PVA hybrid membranes for ethanol dehydration via pervaporation. *Sep. Purif. Technol.* **2018**, *201*, 256–267. [[CrossRef](#)]
34. Jiang, H.J.; Shi, W.X.; Liu, Q.; Wang, H.Y.; Li, J.L.; Wu, C.L.; Li, Y.C.; Wei, Z. Intensification of water/ethanol separation by PVA hybrid membrane with different functional ligand UiO-66-X nanochannels in pervaporation process. *Sep. Purif. Technol.* **2021**, *256*, 117802. [[CrossRef](#)]
35. Kudasheva, A.; Sorribas, S.; Zornoza, B.; Téllez, C.; Coronas, J. Pervaporation of water/ethanol mixtures through polyimide based mixed matrix membranes containing ZIF-8, ordered mesoporous silica and ZIF-8-silica core-shell spheres. *J. Chem. Technol. Biotechnol.* **2015**, *90*, 669–677. [[CrossRef](#)]
36. Liu, Y.; Pan, F.; Wang, M.; Cao, C.; Zhang, Z.; Wang, H.; Liu, X.; Li, Y.; Jiang, Z. Vertically oriented Fe<sub>3</sub>O<sub>4</sub> nanoflakes within hybrid membranes for efficient water/ethanol separation. *J. Membr. Sci.* **2021**, *620*, 118916. [[CrossRef](#)]
37. Selim, A.; Toth, A.J.; Fozer, D.; Szanyi, A.; Mizsey, P. Pervaporative dehydration of methanol using PVA/nanoclay mixed matrix membranes: Experiments and modeling. *Membranes* **2020**, *10*, 435. [[CrossRef](#)]
38. Liu, G.; Jin, W.; Xu, N. Graphene-based membranes. *Chem. Soc. Rev.* **2015**, *44*, 5016–5030. [[CrossRef](#)] [[PubMed](#)]
39. Guan, K.; Liu, G.; Matsuyama, H.; Jin, W. Graphene-based membranes for pervaporation processes. *Chin. J. Chem. Eng.* **2020**, *28*, 1755–1766. [[CrossRef](#)]
40. Cheng, X.; Cai, W.; Chen, X.; Shi, Z.; Li, J. Preparation of graphene oxide/poly (vinyl alcohol) composite membrane and pervaporation performance for ethanol dehydration. *RSC Adv.* **2019**, *9*, 15457–15465. [[CrossRef](#)]
41. Bian, Q.B.; Tian, H.F.; Wang, Y.R.; Liu, Q.; Ge, X.; Rajulu, A.V.; Xiang, A.M. Effect of graphene oxide on the structure and properties of poly (vinyl alcohol) composite films. *Polym. Sci. Ser. A Polym. Phys.* **2015**, *57*, 836–844. [[CrossRef](#)]
42. Zhan, X.; Lu, J.; Xu, H.; Liu, J.; Liu, X.; Cao, X.; Li, J. Enhanced pervaporation performance of PDMS membranes based on nano-sized octa[(trimethoxysilyl)ethyl]-POSS as macro-crosslinker. *Appl. Surf. Sci.* **2019**, *473*, 785–798. [[CrossRef](#)]
43. Zhan, X.; Wang, M.; Gao, T.; Lu, J.; He, Y.; Li, J. A highly selective sorption process in POSS-g-PDMS mixed matrix membranes for ethanol recovery via pervaporation. *Sep. Purif. Technol.* **2020**, *236*, 116238. [[CrossRef](#)]
44. Toth, A.J.; Szilagy, B.; Fozer, D.; Haaz, E.; Selim, A.K.M.; Szori, M.; Viskolcz, B.; Mizsey, P. Membrane Flash Index: Powerful and Perspicuous Help for Efficient Separation System Design. *ACS Omega* **2020**, *5*, 15136–15145. [[CrossRef](#)] [[PubMed](#)]
45. Toth, A.J.; Haaz, E.; Valentinyi, N.; Nagy, T.; Tarjani, A.J.; Fozer, D.; Andre, A.; Khaled Mohamed, S.A.; Solti, S.; Mizsey, P. Selection between Separation Alternatives: Membrane Flash Index (MFLI). *Ind. Eng. Chem. Res.* **2018**, *57*, 11366–11373. [[CrossRef](#)]
46. Xue, Y.; Liu, Y.; Lu, F.; Qu, J.; Chen, H.; Dai, L. Functionalization of graphene oxide with polyhedral oligomeric silsesquioxane (POSS) for multifunctional applications. *J. Phys. Chem. Lett.* **2012**, *3*, 1607–1612. [[CrossRef](#)] [[PubMed](#)]
47. Hayyan, M.; Abo-Hamad, A.; AlSaadi, M.A.; Hashim, M.A. Functionalization of graphene using deep eutectic solvents. *Nanoscale Res. Lett.* **2015**, *10*, 324. [[CrossRef](#)] [[PubMed](#)]
48. Kashyap, S.; Pratihari, S.K.; Behera, S.K. Strong and ductile graphene oxide reinforced PVA nanocomposites. *J. Alloys Compd.* **2016**, *684*, 254–260. [[CrossRef](#)]
49. Shameli, A.; Ameri, E. Synthesis of cross-linked PVA membranes embedded with multi-wall carbon nanotubes and their application to esterification of acetic acid with methanol. *Chem. Eng. J.* **2017**, *309*, 381–396. [[CrossRef](#)]
50. Xia, L.L.; Li, C.L.; Wang, Y. In-situ crosslinked PVA/organosilica hybrid membranes for pervaporation separations. *J. Membr. Sci.* **2016**, *498*, 263–275. [[CrossRef](#)]
51. Le, N.L.; Wang, Y.; Chung, T.S. Pebax/POSS mixed matrix membranes for ethanol recovery from aqueous solutions via pervaporation. *J. Membr. Sci.* **2011**, *379*, 174–183. [[CrossRef](#)]
52. Sun, D.; Li, B.B.; Xu, Z.L. Pervaporation of ethanol/water mixture by organophilic nano-silica filled PDMS composite membranes. *Desalination* **2013**, *322*, 159–166. [[CrossRef](#)]